Electronic Supplementary Material (ESI) for Journal of Materials Chemistry C.

Supporting Materials

Self-trap-state adjustable Photoluminescence of Quasi-One-Dimensional $RbPbI_3$ and Cs Substitutional Counterparts

Bin-Bin Zhang,[*,a] Fangbao Wang,[a] Bao Xiao,[a] Yadong Xu,[a] Kaige Gao,[b] and Wanqi Jie[a]

[a] *State Key Laboratory of Solidification Processing & Key Laboratory of Radiation Detection Materials and Devices, School of Materials Science and Engineering, Northwestern Polytechnical University, Xi'an 710072, China.*

[a] *College of Physical Science and Technology, Yangzhou University, Yangzhou 225009, China*

Corresponding Author:

*E-mail address: zbb@nwpu.edu.cn (B.-B. Zhang).

1. The crystal growth and the component of $Rb_xCs_{1-x}PbI_3$.

$(Rb_xCs_{1-x})PbI_3$ crystals were grown from hydroiodic acid (HI) aqueous solution, which was similar to the growth process of the $RbPbI_3$ crystals in the main text. In order to adjust the value of *x*, the mole ratio of the starting components RbI (99.99%, Sigma-Aldrich) and CsI (99.99%, Sigma-Aldrich) were controlled from 1:0, 2:1, 1:1 to 0:1, as shown in Table S1.

A series of merdoie rod-like $(Rb_xCs_{1-x})PbI_3$ crystals (x=1, 0.34, 0.24 and 0) were obtained. It is noted that the solubility of RbI in hydroiodic acid (HI) aqueous solution is larger than that of CsI and more content of RbI should be added into the HI solution in order to increase the final value of *x*. The energy-dispersive spectroscopy (EDS) in Fig. S1 reveals the intensity of the peak for Rb (at 1.8 keV) is gradually enhanced with increasing the content of RbI in the starting materials.

Table S1. The mole ratio of the starting materials RbI and CsI for the preparation of $(Rb_xCs_{1-x})PbI_3$ crystals and the corresponding final *x* value.

n(RbI) : n(CsI)	*x*
1:0	1
2:1	0.34
1:1	0.24
0:1	0

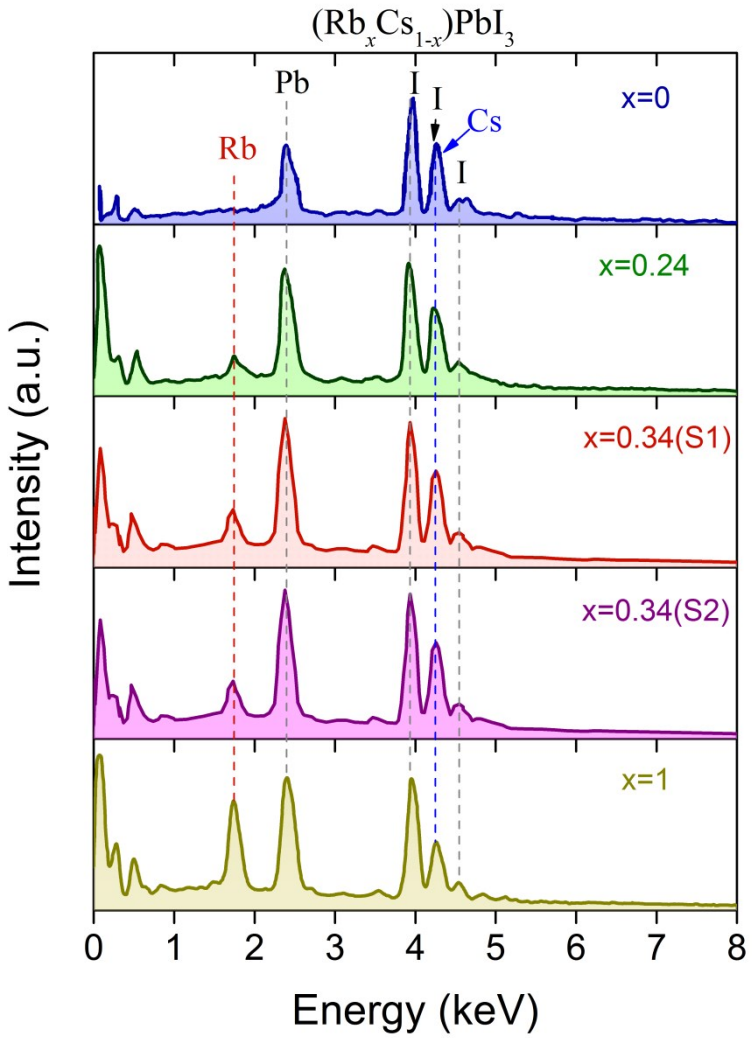

Fig. S1 The energy-dispersive spectroscopy (EDS) of $(Rb_xCs_{1-x})PbI_3$ (x=0, 0.24, 0.34, and 1).

2. The crystal structures of $(Rb_xCs_{1-x})PbI_3$

The crystal structures of $(Rb_xCs_{1-x})PbI_3$ were also changed with the variable value of x. The similar XRD patterns of $(Rb_xCs_{1-x})PbI_3$ (x=0, 0.24, 0.34 and 1) are shown in Fig. S2(a). It indicates they have similar crystal structure (Fig. S2(b)) and all belong to the same space group *Pnma*.[1, 2] With the Rb content increasing, the peaks of (0 0 2) and (1 0 2) move to higher angles, implying a shrinkage of the lattice structure.

The lattice constants obtained from the Rietveld refinement are a = 10.46 Å, b = 4.80 Å, c = 17.78 Å for $CsPbI_3$ (x=0), respectively. As the Rb atoms with smaller radius entered into crystal lattice, the lattice parameters a, b and c reduced monotonically with increased value of x, as revealed in Fig. S2(c).

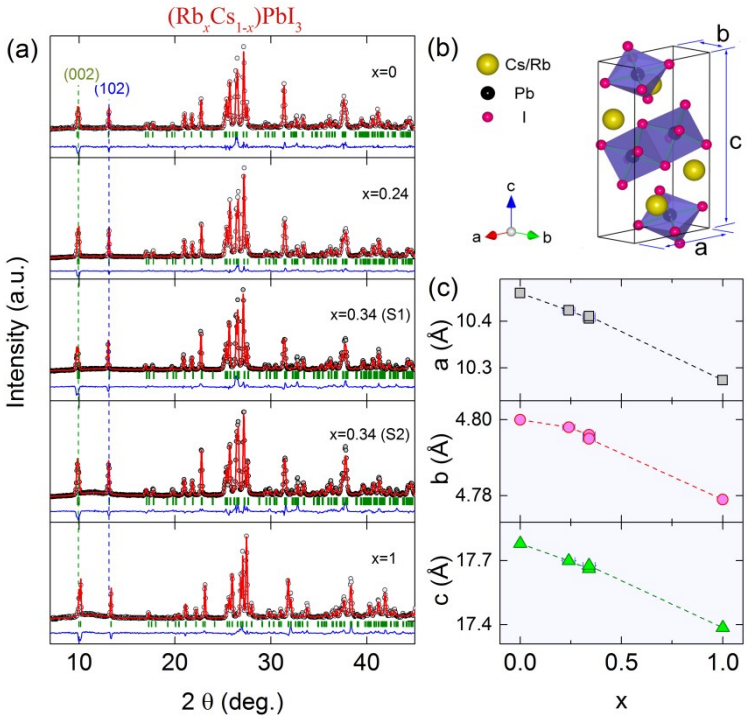

Fig. S2 (a) The Rietveld refinement of the powder XRD patterns of $(Rb_xCs_{1-x})PbI_3$ (x=0, 0.24, 0.34 and 1). (b) Crystal structure of $(Rb_xCs_{1-x})PbI_3$ crystals. (c) The lattice parameters deceased with the increasing value of x.

Table S2. The Goodness of fit and the atomic refinement parameters of $(Rb_xCs_{1-x})PbI_3$ (x=0, 0.24, 0.34 and 1).

x	$_WR_P$	R_F		x	y	z
0	10.3%	8.6%	Cs	0.082131	0.750000	0.328651
			Pb	0.161756	0.250000	0.062564
			I1	0.036021	0.250000	0.879353
			I2	0.159441	0.250000	0.495688

			I3	0.199228	0.750000	0.715874
x	$_{W}R_{P}$	R_F		*x*	*y*	*z*
0.24	9.1%	5.9%	Rb	0.082853	0.750000	0.328600
			Cs	0.082853	0.750000	0.328600
			Pb	0.162062	0.250000	0.062656
			I1	0.031315	0.250000	0.881379
			I2	0.160233	0.250000	0.495615
			I3	0.198964	0.750000	0.715581
x	$_{W}R_{P}$	R_F		*x*	*y*	*z*
0.34 (S1)	13.5%	11.0%	Rb	0.080597	0.750000	0.328447
			Cs	0.080597	0.750000	0.328447
			Pb	0.164855	0.250000	0.063127
			I1	0.032903	0.250000	0.878669
			I2	0.155840	0.250000	0.493691
			I3	0.198695	0.750000	0.717625
x	$_{W}R_{P}$	R_F		*x*	*y*	*z*
0.34 (S2)	12.6%	10.5%	Rb	0.080995	0.750000	0.328247
			Cs	0.080995	0.750000	0.328247
			Pb	0.163699	0.250000	0.063019
			I1	0.034498	0.250000	0.880295
			I2	0.158467	0.250000	0.494155
			I3	0.197235	0.750000	0.715914
x	$_{W}R_{P}$	R_F		*x*	*y*	*z*
1	11.9%	9.9%	Rb	0.083371	0.750000	0.323161
			Pb	0.167975	0.250000	0.060429
			I1	0.031478	0.250000	0.879301
			I2	0.155923	0.250000	0.489312
			I3	0.190449	0.750000	0.718226

3. The reflection spectra and band gaps of $(Rb_xCs_{1-x})PbI_3$

As shown in Fig. S3(a), UV-Vis diffuse reflectance measurement ranged from 350 to 700 nm was performed at room temperature to determine the bandgap of $(Rb_xCs_{1-x})PbI_3$ crystals. Sharp decreases in reflectance at about 500 nm were observed for the samples due to the strong absorption. The reflectance spectra can be analyzed

by converting reflectance into absorbance data according to the Kubelka-Munk function[3]:

$$F(R)=\frac{\alpha}{S}=\frac{(1-R)^2}{2R}\sim\alpha \qquad \text{* MERGEFORMAT (1)}$$

where R is the relative reflectance ratio, α is the absorption coefficient of the sample, and S is the scattering coefficient. Fig. S3(b) shows the Kubelka-Munk absorption spectra (α/S) of the $(Rb_xCs_{1-x})PbI_3$ crystal. By extrapolating the linear portion of the absorbance vs. energy to zero absorption, the obtained band gaps (Eg) are exhibited in Fig. S3(c).

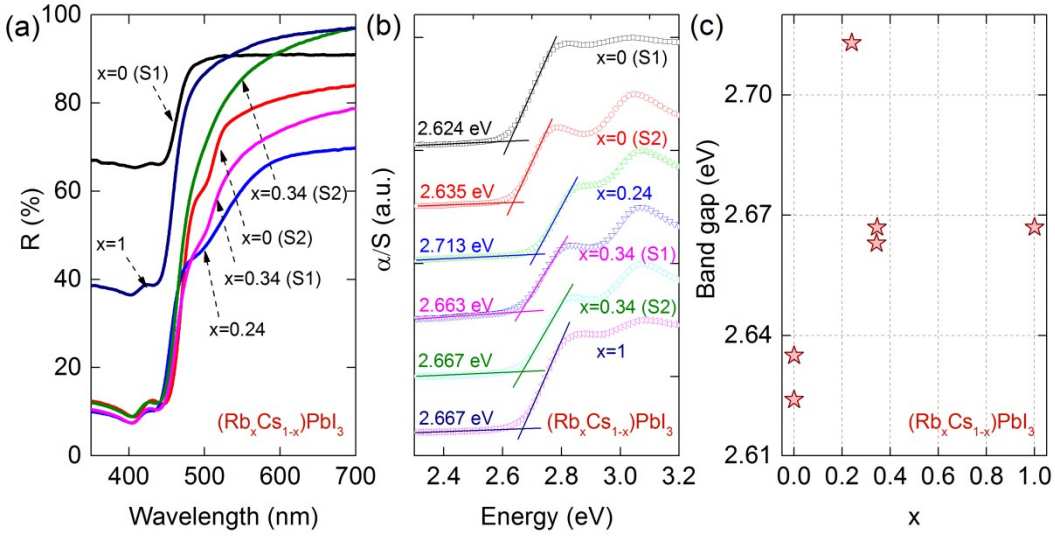

Fig. S3. (a) The UV-Vis diffuse reflectance spectra of $(Rb_xCs_{1-x})PbI_3$ powders. (b) The absorbance spectra derived by the Kubelka-Munk function. (c) The calculated band gap of $(Rb_xCs_{1-x})PbI_3$.

4. The power and temperature dependent photoluminescence of $(Rb_xCs_{1-x})PbI_3$ (x=0, 0.24, 0.34(S1) and 0.34(S2)) crystals

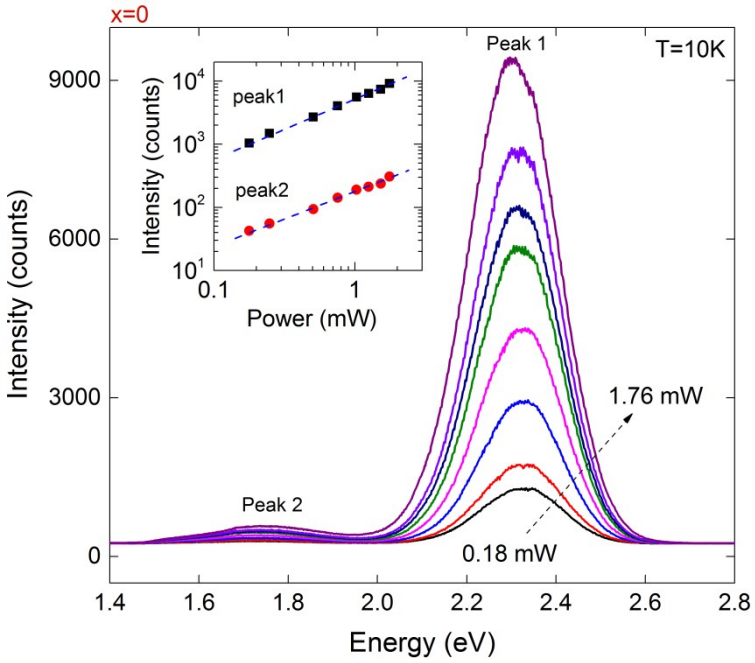

Fig. S4. The power dependent photoluminescence of $CsPbI_3$ crystal from 0.18 mW to 1.76 mW. The inset shows the PL intensity versus incident power data with a linear correlation.

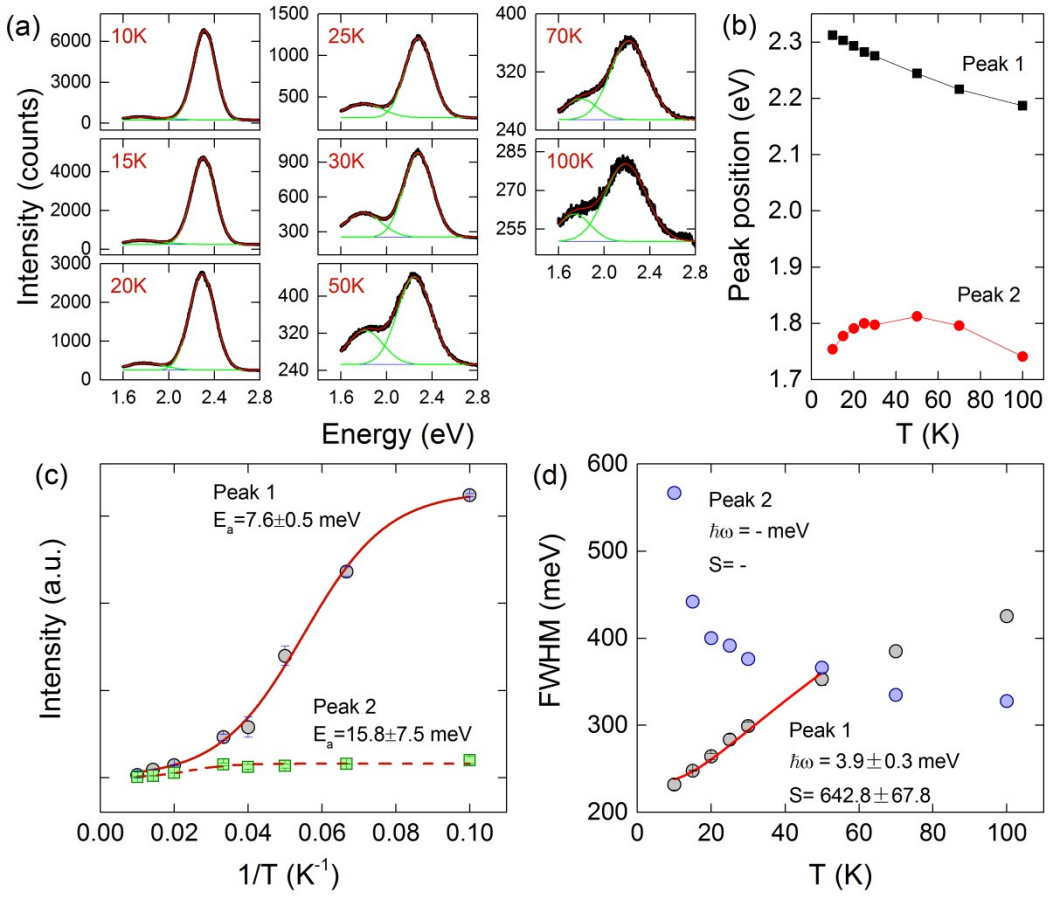

Fig. S5. (a) The temperature dependent photoluminescence of $CsPbI_3$ crystal from 10 K to 100 K. (b) The PL peaks location of $CsPbI_3$ crystal in different temperature. (c) The intensity of PL peaks of $CsPbI_3$ crystal in different temperature and the calculated dissociation energies obtained by fitting the data with the formula $I(T) = \frac{I(0)}{1 + C \cdot \exp(-E/kT)}$. (d) The full width half maximum (FWHM) of PL peaks of $CsPbI_3$ crystal in different temperature and the S and $\hbar\omega$ obtained by fitting the data.

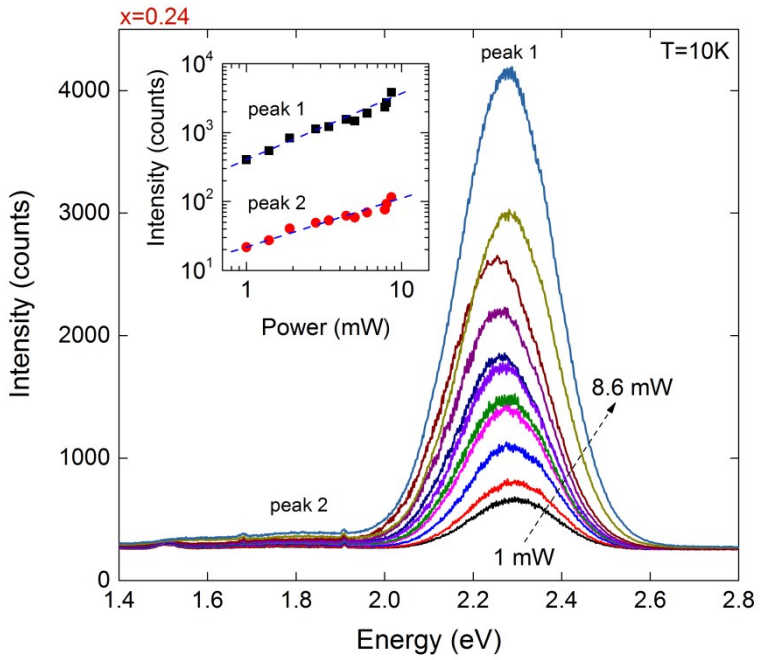

Fig. S6. The power dependent photoluminescence of $(Rb_{0.24}Cs_{0.76})PbI_3$ crystal from 1 mW to 8.6 mW. The inset shows the PL intensity versus incident power data with a linear correlation.

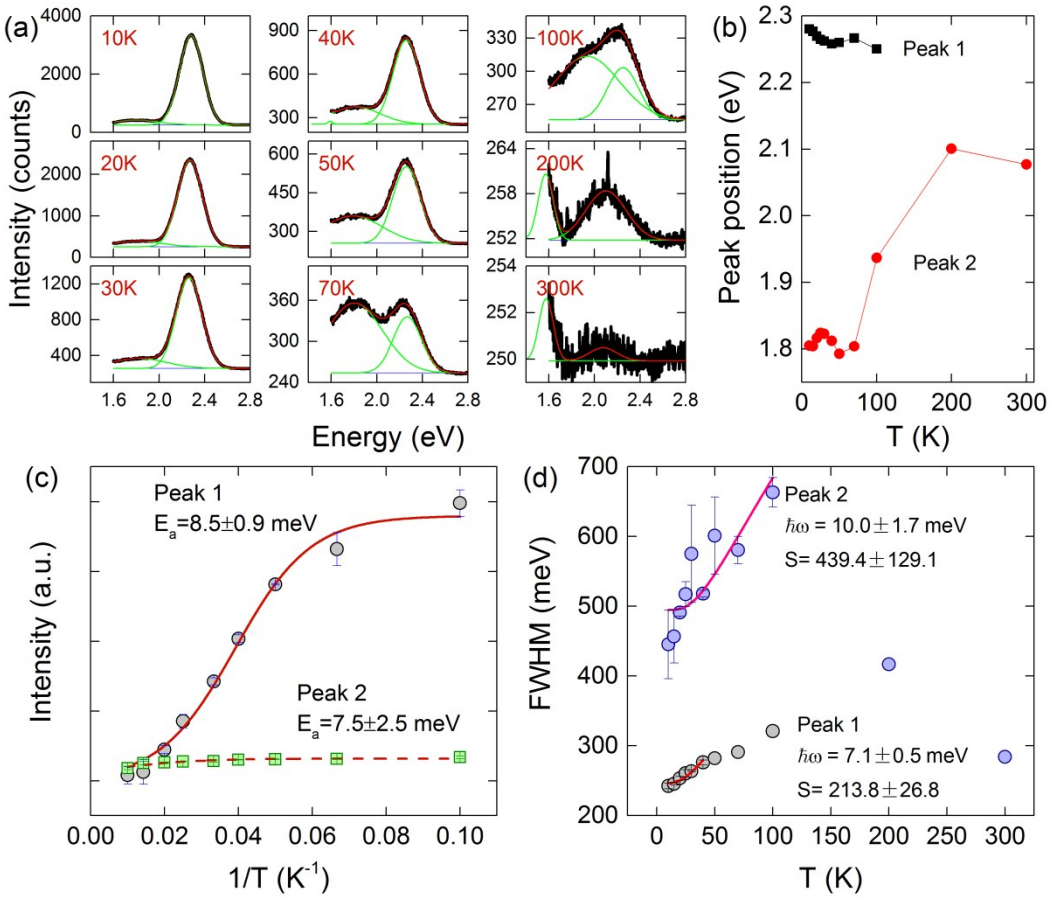

Fig. S7. (a) The temperature dependent photoluminescence of $(Rb_{0.24}Cs_{0.76})PbI_3$ crystal from 10 K to 300 K. (b) The PL peaks location of $(Rb_{0.24}Cs_{0.76})PbI_3$ crystal in different temperature. (c) The intensity of PL peaks of $(Rb_{0.24}Cs_{0.76})PbI_3$ crystal in different temperature and the calculated dissociation energies obtained by fitting the data with the formula $I(T) = \frac{I(0)}{1 + C \cdot \exp(-E / kT)}$. (d) The full width half maximum (FWHM) of PL peaks of $(Rb_{0.24}Cs_{0.76})PbI_3$ crystal in different temperature and the S and $\hbar\omega$ obtained by fitting the data.

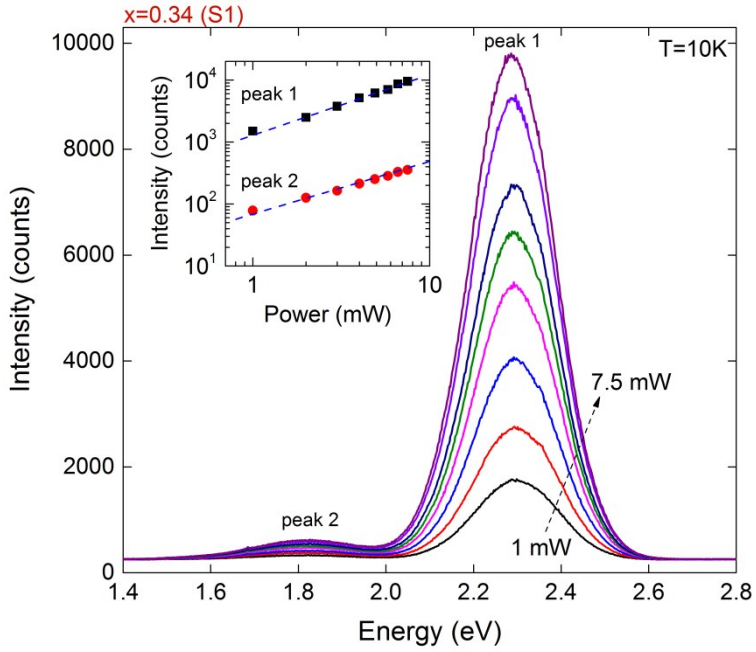

Fig. S8. The power dependent photoluminescence of $(Rb_{0.34}Cs_{0.66})PbI_3$ (S1) crystal from 1 mW to 7.5mW. The inset shows the PL intensity versus incident power data with a linear correlation.

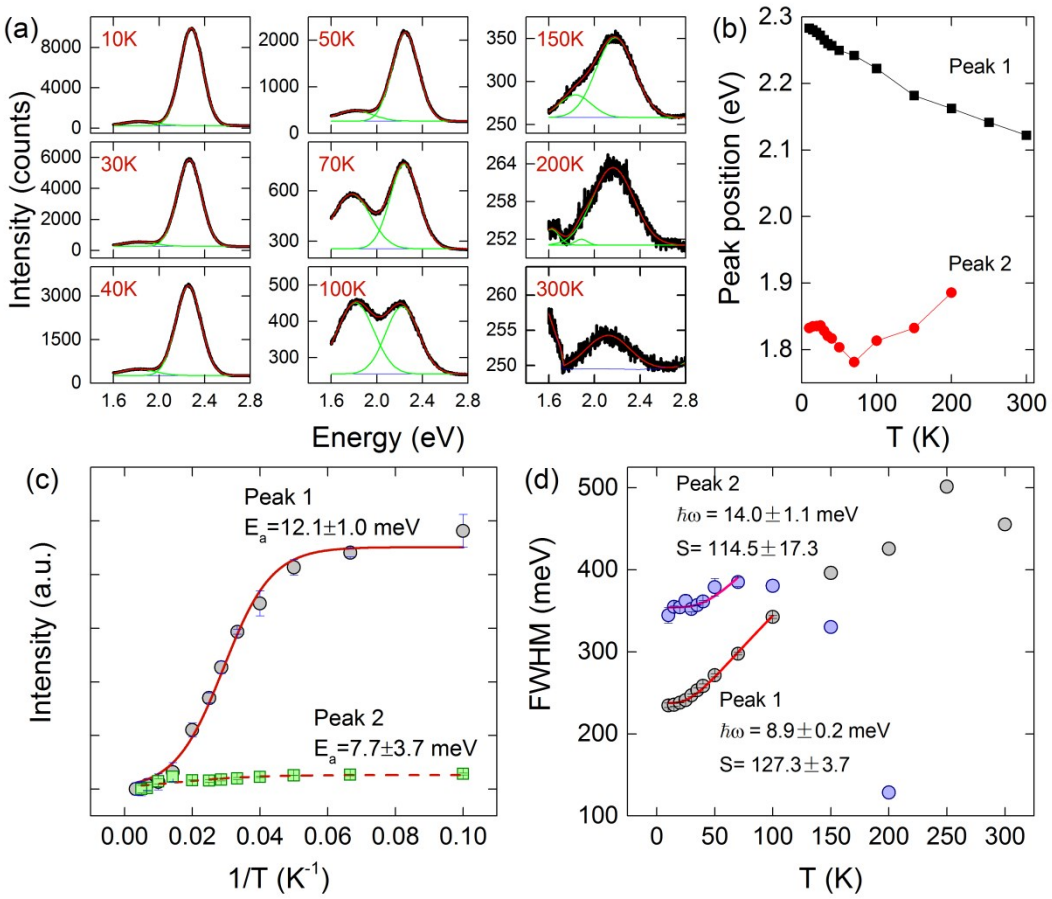

Fig. S9. (a) The temperature dependent photoluminescence of $(Rb_{0.34}Cs_{0.66})PbI_3$ (S1) crystal from 10 K to 300 K. (b) The PL peaks location of $(Rb_{0.34}Cs_{0.66})PbI_3$ (S1) crystal in different temperature. (c) The intensity of PL peaks of $(Rb_{0.34}Cs_{0.66})PbI_3$ (S1) crystal in different temperature and the calculated dissociation energies obtained by fitting the data with the formula $I(T) = \frac{I(0)}{1 + C \cdot \exp(-E/kT)}$. (d) The full width half maximum (FWHM) of PL peaks of $(Rb_{0.34}Cs_{0.66})PbI_3$ (S1) crystal in different temperature and the S and $\hbar\omega$ obtained by fitting the data.

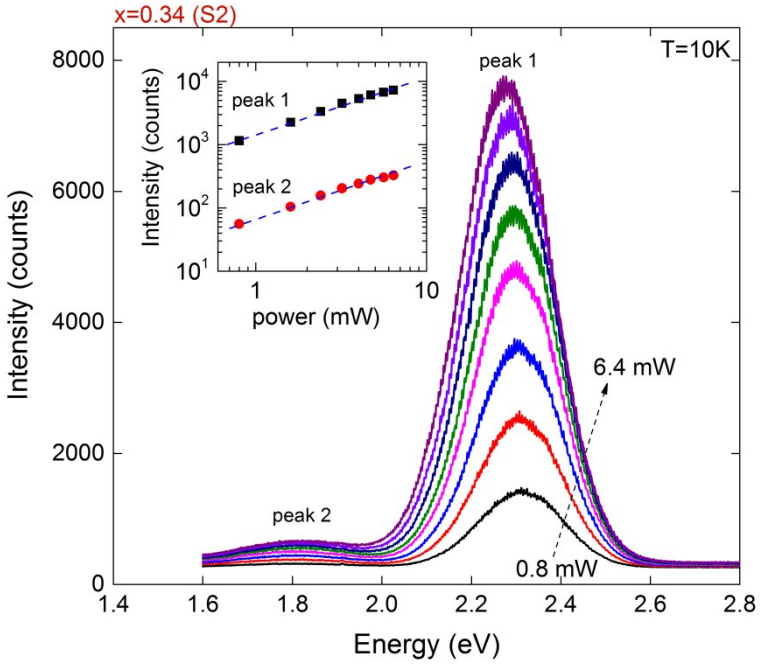

Fig. S10. The power dependent photoluminescence of $(Rb_{0.34}Cs_{0.66})PbI_3$ (S2) crystal from 0.8 mW to 6.4 mW. The inset shows the PL intensity versus incident power data with a linear correlation.

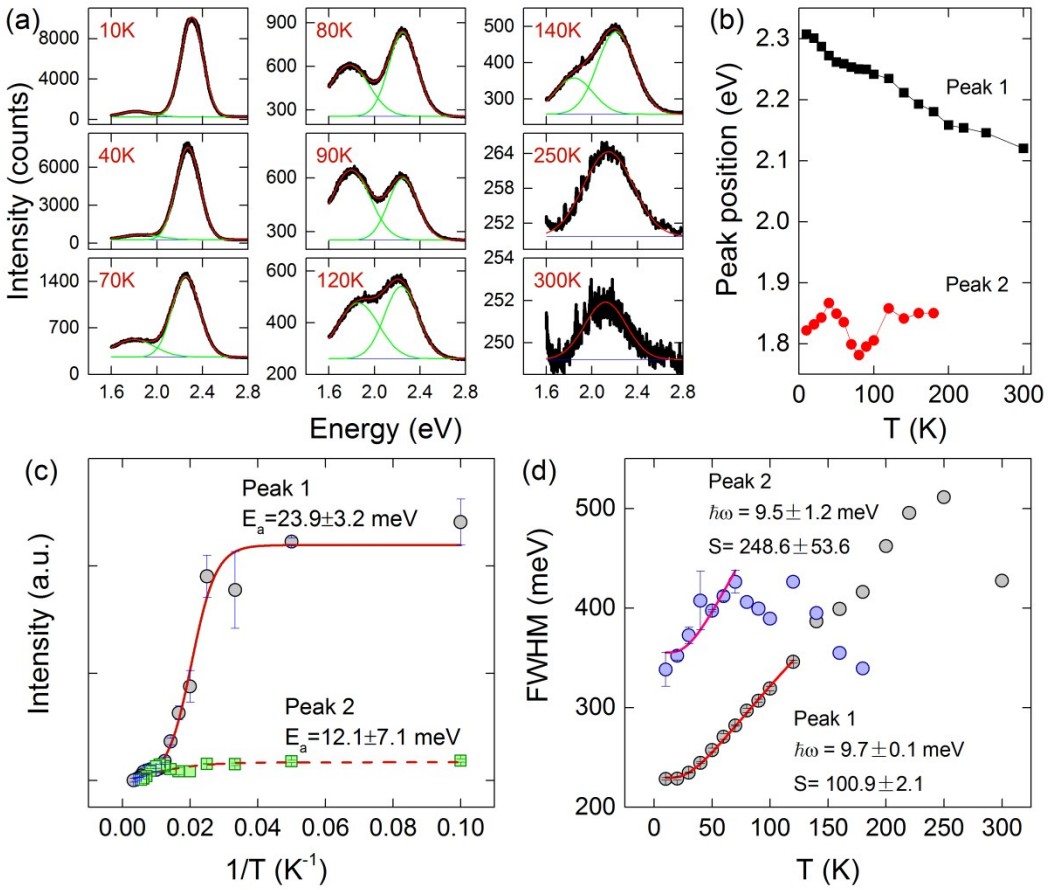

Fig. S11. (a) The temperature dependent photoluminescence of $(Rb_{0.34}Cs_{0.66})PbI_3$ (S2) crystal from 10 K to 300 K. (b) The PL peaks location of $(Rb_{0.34}Cs_{0.66})PbI_3$ (S2) crystal in different temperature. (c) The intensity of PL peaks of $(Rb_{0.34}Cs_{0.66})PbI_3$ (S2) crystal in different temperature and the calculated dissociation energies obtained by fitting the data with the formula $I(T) = \frac{I(0)}{1 + C \cdot \exp(-E/kT)}$. (d) The full width half maximum (FWHM) of PL peaks of $(Rb_{0.34}Cs_{0.66})PbI_3$ (S2) crystal in different temperature and the S and $\hbar\omega$ obtained by fitting the data.

5. The stability of $(Rb_xCs_{1-x})PbI_3$ single crystals

As shown in Fig. S12, the XRD patterns of $(Rb,Cs)PbI_3$ crystal samples were tested again after 21 month store in atmospheric environment. In comparisons to our

initial tests, no obvious differences and other phases were observed. Therefore, the inorganic $(Rb,Cs)PbI_3$ crystal samples reveals strong stability in atmospheric environment.

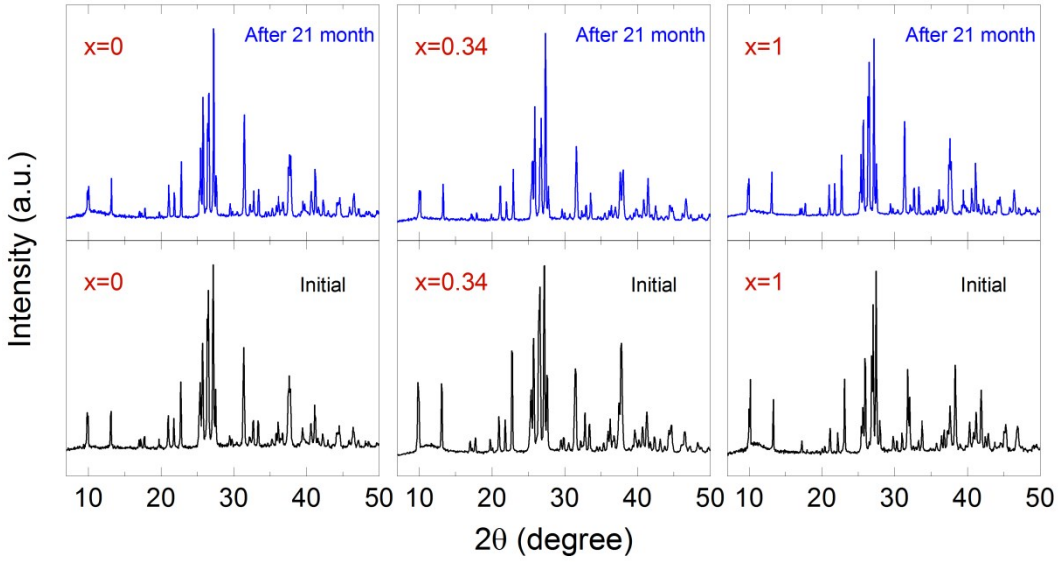

Fig. S12. The XRD patterns of $(Rb_xCs_{1-x})PbI_3$ crystal samples before and after 21 month store in atmospheric environment.

References:

1. B.-B. Zhang, B. Xiao, S. Dong and Y. Xu, *J. Cryst. Growth*, 2018, **498**, 1-4.
2. D. H. Lim, P. Ramasamy, D. H. Kwak and J. S. Lee, *Nanotechnology*, 2017, **28**, 255601.
3. B. Xiao, M. Q. Zhu, L. L. Ji, B. B. Zhang, J. P. Dong, J. Y. Yu, Q. H. Sun, W. Q. Jie and Y. D. Xu, *Journal of Crystal Growth*, 2019, **517**, 7-11.